RESEARCH MEMORANDUM

PRESSURE DISTRIBUTION OVER A SHARP-NOSE BODY OF REVOLUTION AT TRANSONIC SPEEDS BY THE NACA WING-FLOW METHOD

By

Edward C. B. Danforth and J. Ford Johnston

Langley Memorial Aeronautical Laboratory
Langley Field, Va.

NATIONAL ADVISORY COMMITTEE FOR AERONAUTICS

WASHINGTON

March 5, 1948

Classification cancelled (or changed to Unclassified)

By authority of NASA Tech. Publication

By (OFFICER AUTHORIZED) 29 Jan 64

By .....

NK

(GRADE OF OFFICER MAKING CHANGE)

11 Aug 62

DATE

NATIONAL ADVISORY COMMITTEE FOR AERONAUTICS

RESEARCH MEMORANDUM

PRESSURE DISTRIBUTION OVER A SHARP-NOSE BODY OF REVOLUTION AT TRANSONIC SPEEDS BY THE NACA WING-FLOW METHOD

By Edward C. B. Danforth and J. Ford Johnston

SUMMARY

The pressure distribution over a sharp-nose body of revolution having a circular-arc profile and fineness ratio 6 has been obtained at transonic speeds by the NACA wing-flow method.

It was found that the transition from the theoretical subsonic to the theoretical supersonic types of pressure distribution occurred rapidly but smoothly in the Mach number range from 0.92 to 1.00. The corresponding growth and rearward shift of the negative-pressure region caused a rapid rise in the pressure-drag coefficient from 0 at a Mach number of 0.94 to 0.21 at a Mach number of 1.00, and a slower rise thereafter. This pressure drag was not associated with separation.

INTRODUCTION

The over-all aerodynamic characteristics of fuselage-like bodies are currently being studied at transonic speeds by the free-fall method (references 1 and 2) and rocket method (reference 3). It is desirable to supplement these investigations by the measurement of the pressure distribution in order to obtain a more detailed understanding of the flow characteristics.

Exploratory pressure distributions, presented herein, have been obtained at transonic speeds over a body of revolution by the NACA wing-flow method. The purpose of the investigation was twofold: to compare the experimental distributions with the theoretical subsonic and supersonic distributions; and to study the manner in which the distribution changed through the transonic range, with particular reference to the causes of the rapid increase in drag.

APPARATUS AND METHOD

Two bodies of revolution having a maximum diameter of 1 inch, fineness ratio 6 to 1, and circular-arc profile were constructed for the investigation. The first body was mounted on a $\frac{1}{2}$-inch-diameter sting which joined the body at 86 percent of the body length. The upper and lower meridian lines carried six orifices each spaced along the length of the body. The second body was mounted on a $\frac{1}{4}$-inch-diameter sting which joined the body at 94 percent of the length. The orifices on this body were concentrated in the rear, four orifices on the upper meridian and two on the lower meridian. Photographs of the bodies are shown in figures 1 and 2 and sketches showing dimensions and orifice locations are shown as figure 3. The body-sting combinations were mounted $6\frac{1}{2}$ inches above the airplane wing, as shown in figure 4, and were alined laterally with the local flow direction.

The experimental technique, which followed the general method of reference 4, was to dive the airplane from an altitude of 28,000 feet and a Mach number of 0.50 to 15,000 feet and a Mach number of 0.72. The corresponding variation of Mach number at the model position was from 0.65 to 1.08 and the Reynolds number based on the body length of 6 inches varied from 0.80×10^6 to 1.60×10^6. During the dive, standard NACA instruments continuously recorded and synchronized all model pressures, airplane impact and static pressures, free air temperature, and normal acceleration.

The chordwise variation of wing surface Mach number M_s along the test section, determined from flights without a model, is shown in figure 5. The Mach number M at the height of the model was calculated from the predetermined normal gradient, the value of which averaged about $-0.007M_s$ per inch away from the surface. The Mach numbers quoted in the remainder of the report are the average values over the length of the body. The dynamic pressure and reference static pressure used in the calculation of the pressure coefficient $\Delta p/q$ correspond to this average Mach number.

RESULTS AND DISCUSSION

Variation of pressure coefficient with Mach number.- The variation of pressure coefficient $\Delta p/q$ with Mach number M is shown for each orifice position x/l (see fig. 3) in figures 6 and 7 for the body with the large sting ($\frac{1}{2}$-inch diameter) and with the small sting ($\frac{1}{4}$-inch diameter), respectively. The curvature of the flow over the airplane wing was such as to put the nose of the bodies at about 1° angle of attack. Examination of parts (a), (b), and (c) of figure 6

will show the effect of this angle of attack in that the pressures on the upper meridian are more negative than those on the lower meridian. Theoretical calculations based on reference 5 and independent of Mach number to the first order indicate pressure differences due to 1° angle of attack of about the same magnitude as those measured. The more rearward orifices, parts (d), (e), and (f) of figure 6, show only small angle-of-attack effects. Evidently the rear of the body was very nearly alined with the flow. The angle-of-attack effect on the measured pressures should also be small for the body with the small sting, since the orifices were all toward the rear of the body.

In figure 6 there is also plotted for each orifice position the variation of $\Delta p/q$ with M which was obtained by applying the three-dimensional Prandtl-Glauert corrections (references 6 and 7) to the theoretical incompressible pressures calculated from thin-body theory for the body-sting combination. The compressibility corrections of references 6 and 7 are strictly applicable only near the maximum diameter of an ellipsoid of revolution. Comparisons are made, however, for all orifice positions to examine the general applicability of the corrections. It is seen in figure 6 that the theoretical variation of $\Delta p/q$ with M is in fair agreement with the experimental variation not only at maximum thickness (fig. 6(d)) but at points both forward of and behind maximum thickness, except very near the nose of the body (fig. 6(a)). The theoretical variation tended to overestimate the changes of $\Delta p/q$ with M for positive pressures and underestimate the changes for negative pressures.

On the forward part of the body (figs. 6(a), 6(b), and 6(c)), the experimental variation of pressure with Mach number is always small and continuous. Near midlength and in the rear, however, (figs. 6(d), 6(e), and 6(f) and fig. 7) the changes in pressure are large and abrupt between $M = 0.92$ and $M = 1.05$. These large abrupt changes are associated with the rapid growth and the rearward shift of the peak negative pressures in this Mach number range. Although the changes in the individual pressures are abrupt, it will be shown that the pressure distribution as a whole changes shape smoothly.

Pressure distributions along the body axis.- The distribution of pressure along the body axis is shown for several Mach numbers in figure 8 for the body with the large sting. The experimental points show the average pressure between the upper and lower meridians, and thus represent closely the condition of zero angle of attack. These averaged distributions are compared with the theoretical incompressible and theoretical compressible distributions.

At $M = 0.70$ (fig. 8(a)) the experimental points agree closely with the incompressible distribution. It would appear that the effect of compressibility on the body pressures is slight at Mach numbers of 0.70 and below.

[redacted]

At Mach numbers of 0.80, 0.90, and 0.92 (figs. 8(b), 8(c), and 8(d)) the pressures are definitely increased in absolute magnitude over the incompressible values. The theoretical compressible distributions at these Mach numbers are in reasonable agreement with the experimental distributions except near the nose.

The distribution for $M = 0.92$ (fig. 8(d)) shows that slightly supersonic speeds are here attained over the thicker parts of the body. The attainment of sonic speeds seems to be a point of demarcation as far as the general shape of the pressure distributions is concerned. Below $M = 0.92$ the experimental distributions are symmetrical, except for the asymmetry induced by the presence of the sting, and the growth of the pressures with Mach number is relatively slow. Between $M = 0.92$ and $M = 1.00$, however, (figs. 8(d) to 8(g)) the peak negative pressures grow rapidly and the negative pressure region shifts rapidly rearward.

As the Mach number becomes supersonic (figs. 8(h), 8(i), and 8(j)) the rearward movement of the peak negative pressures becomes less pronounced, the peak pressures themselves tend to decrease in magnitude, and the pressure distribution approaches the type found theoretically in reference 8.

Theoretical distributions calculated from reference 8 are compared in figure 8(j) with the experimental distribution for $M = 1.05$. The experimental and theoretical distributions for $M = 1.05$ are in fair agreement although the assumptions of the linearized theory are generally not believed valid for Mach numbers so near unity. Theoretical distributions for Mach numbers of 1.15 and 1.4 are also presented to indicate the changes in distribution to be expected above $M = 1.05$. These changes are in line with those observed between $M = 1.00$ and $M = 1.05$. It is interesting that the rapid pressure recovery over the rear of the body that is predicted theoretically is evidenced in the experimental data without any sensible flow separation at least to $\frac{x}{l} = 0.83$ in spite of the severe adverse pressure gradients encountered and the small scale of the tests.

In order to study further the problems of flow separation, a second body was constructed with a smaller sting and with pressure orifices concentrated over the rear part. The lengthwise pressure distributions for this body are shown in figure 9. At each Mach number the fairing between $\frac{x}{l} = 0$ and $\frac{x}{l} = 0.50$ was taken from figure 8 inasmuch as neither sting can have appreciable effect on the body pressures ahead of $\frac{x}{l} = 0.50$.

The distribution of pressures behind $\frac{x}{l} = 0.83$ (figs. 9(a) to 9(g)) shows a slight tendency toward separation. This condition becomes aggravated as the Mach number increases from 0.70 to 0.98. At a Mach number of 1.00 and above (figs. 9(h), 9(i), and 9(j)) the pressure recovery takes place continuously to the last point of measurement $\left(\frac{x}{l} = 0.91\right)$, and good agreement is obtained between the theoretical and experimental rear pressure recoveries at $M = 1.05$. It appears likely that for a complete body (no sting) no important flow separation would occur forward of $\frac{x}{l} = 0.91$. Any separation occurring behind $\frac{x}{l} = 0.91$ would, since the cross section is small, have only a small effect on the drag.

Pressure drag.- Sample curves of $\Delta p/q$ against $(r/R)^2$ (see fig. 3) for the body with the large sting are shown for $M = 0.70$ and $M = 1.05$ in figure 10. The area enclosed by such a curve is, with proper regard to sign, equal to the drag coefficient C_D of the body-sting combination, based on frontal area. At $M = 0.70$ (fig. 10(a)) the net drag of the combination is very nearly zero as would be expected from considerations of subsonic potential flow. At $M = 1.05$ (fig. 10(b)), however, a net drag force exists.

The variation of pressure-drag coefficient with Mach number for the two body-sting combinations shows a striking resemblance (fig. 11) to the variation of total-drag coefficient (reference 1) for a freely falling body of the same fineness ratio. The pressure-drag coefficient increases sharply from zero at $M = 0.94$ to about 0.21 at $M = 1.00$ and increases less sharply above $M = 1.00$ reaching a value of about 0.25 at $M = 1.05$. The sharp increase in C_D between $M = 0.94$ and $M = 1.00$ is not associated with any important flow separation, but is due primarily to the rapid growth and rearward shift of the negative pressure region as sonic speed is approached. It has already been shown that above $M = 1.00$ the rearward movement of the negative pressure peak is less rapid and that the peak pressures themselves tend to decrease in magnitude. This combined effect results in a less rapid increase of C_D above $M = 1.00$.

Effects of interference and horizontal gradient.- There are two factors that may have affected the measured pressure distributions of the bodies; the interference effect between the body and the airplane wing surface, and the effect of negative pressure gradient along the test section at Mach numbers greater than about 1.0.

Calculations made from the subsonic theory indicate a negligible interference effect to be expected at the lower Mach numbers investigated ($M = 0.70$ and 0.80). At a given x/l (fig. 6) the difference in

pressure between the upper and lower meridians does not vary appreciably with Mach number. This indicates that the effect of interference at the higher Mach numbers was of the same order as that at the lower Mach numbers, and should, therefore, be small.

The falling pressures along the test section at the higher Mach numbers tend to cause a relative decrease in the pressures over the body from the nose to the tail, to cause the negative peak to move slightly more rearward, and, consequently, cause an apparent increase in drag. The adverse pressure gradient near the rear of the body would tend to be reduced and possibly move the point of separation nearer the tail. The effect on the position of the negative peak and on the point of separation should be quite small, however, since the pressure gradient along the test section is small with respect to those on the body.

It is therefore believed that any distortion of the pressure distribution due to the effects of interference or pressure gradient was not of sufficient magnitude to alter the conclusions reached in the discussion.

CONCLUSIONS

Pressure distributions over a sharp-nose body of revolution obtained at transonic speeds by the NACA wing-flow method have indicated that:

1. The types of pressure distribution that were obtained at both subsonic and supersonic speeds were those predicted by thin-body theory.

2. The change in the pressure distribution from the subsonic type to the supersonic type was accomplished rapidly but smoothly in the Mach number range from 0.92 to 1.00.

3. Supersonic speeds were first attained over the thicker sections of the body at a Mach number of 0.92. The pressure drag began to increase noticeably at a Mach number of 0.94.

4. The pressure drag coefficient increased rapidly from 0 to 0.21 as the Mach number increased from 0.94 to 1.00, and increased less rapidly thereafter, reaching a value of 0.25 at a Mach number of 1.05.

5. The pressure drag was not due to separation but principally to the growth and rearward shift of the negative pressures as sonic speed was approached and exceeded.

Langley Memorial Aeronautical Laboratory
National Advisory Committee for Aeronautics
Langley Field, Va.

REFERENCES

1. Bailey, F. J., Jr., Mathews, Charles W., and Thompson, Jim Rogers: Drag Measurements at Transonic Speeds on a Freely Falling Body. NACA ACR No. L5E03, 1945.

2. Thompson, Jim Rogers, and Mathews, Charles W.: Total Drag of a Body of Fineness Ratio 12 and Its Stabilizing Tail Surfaces Measured during Free Fall at Transonic Speeds. NACA CB No. L6D08, 1946.

3. Katz, Ellis R.: Results of Flight Tests at Supersonic Speeds to Determine the Effect of Body Nose Fineness Ratio on Body and Wing Drag. NACA RM No. L7B19, 1947.

4. Gilruth, R. R., and Wetmore, J. W.: Preliminary Tests of Several Airfoil Models in the Transonic Speed Range. NACA ACR No. L5E08, 1945.

5. Tsien, Hsue-Shen: Supersonic Flow over an Inclined Body of Revolution. Jour. Aero. Sci., vol. 5, no. 12, Oct. 1938, pp. 480-483.

6. Lees, Lester: A Discussion of the Application of the Prandtl-Glauert Method to Subsonic Compressible Flow over a Slender Body of Revolution. NACA TN No. 1127, 1946.

7. Hess, Robert V., and Gardner, Clifford S.: Study by the Prandtl-Glauert Method of Compressibility Effects and Critical Mach Number for Ellipsoids of Various Aspect Ratios and Thickness Ratios. NACA RM No. L7B03a, 1947.

8. Jones, Robert T., and Margolis, Kenneth: Flow over a Slender Body of Revolution at Supersonic Velocities. NACA TN No. 1081, 1946.

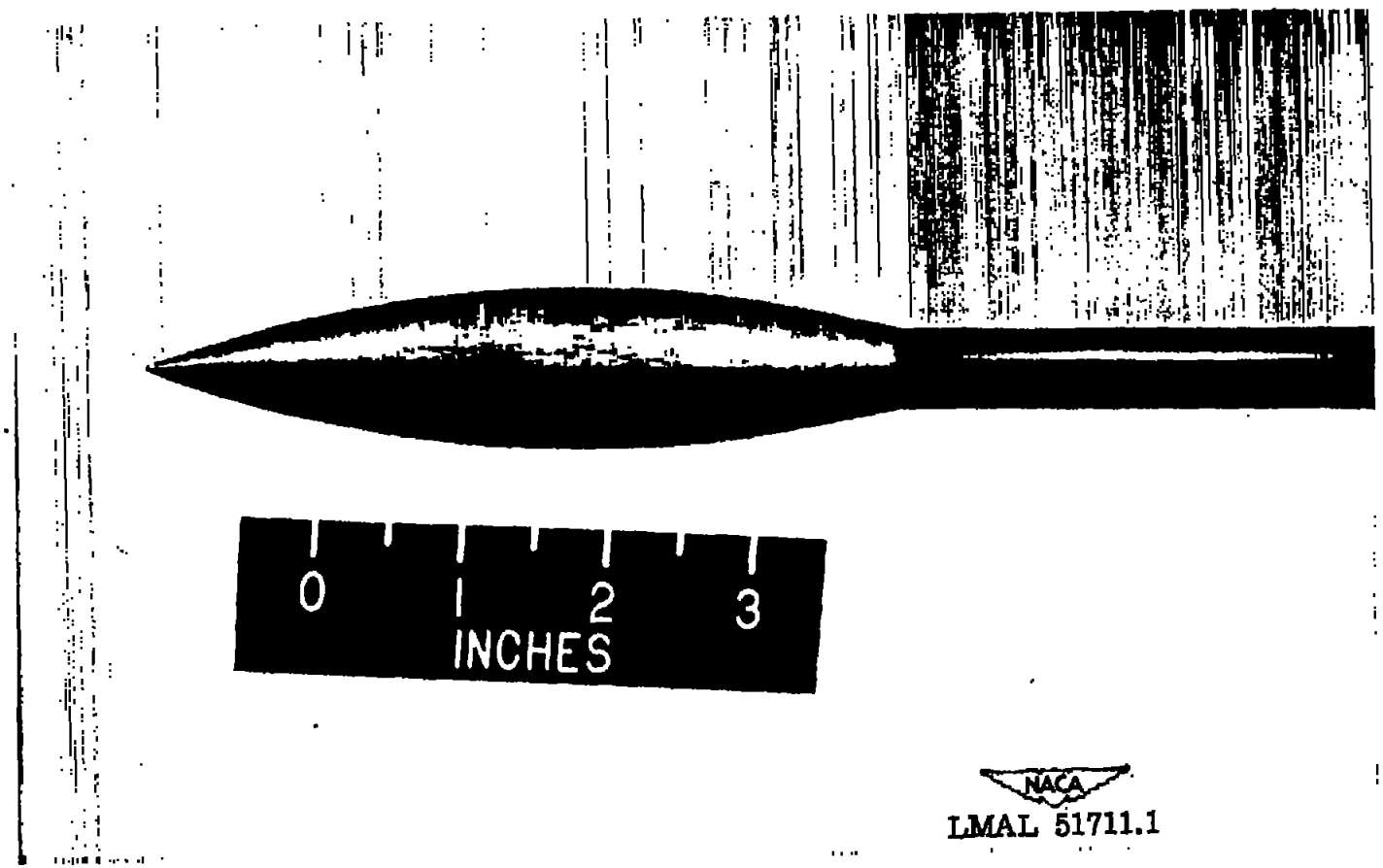

Figure 1.- Body with $\frac{1}{2}$-inch diameter sting.

Figure 2.- Body with $\frac{1}{4}$-inch diameter sting.

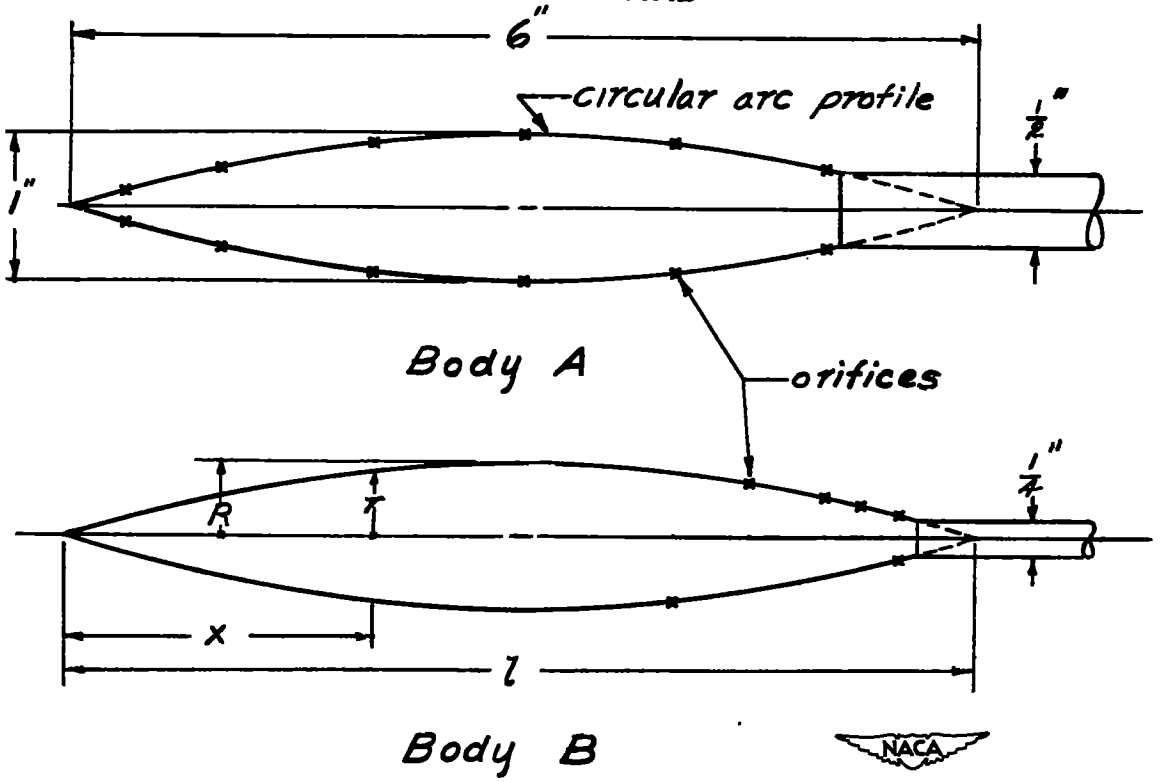

orifice locations, body A

$\frac{x}{l}$	Meridian
.06	upper and lower
.17	" " "
.33	" " "
.50	" " "
.67	" " "
.83	" " "

orifice locations, body B

$\frac{x}{l}$	Meridian
.67	lower
.75	upper
.83	upper
.87	upper
.91	upper and lower

Figure 3.- Sketch of bodies showing dimensions and orifice locations.

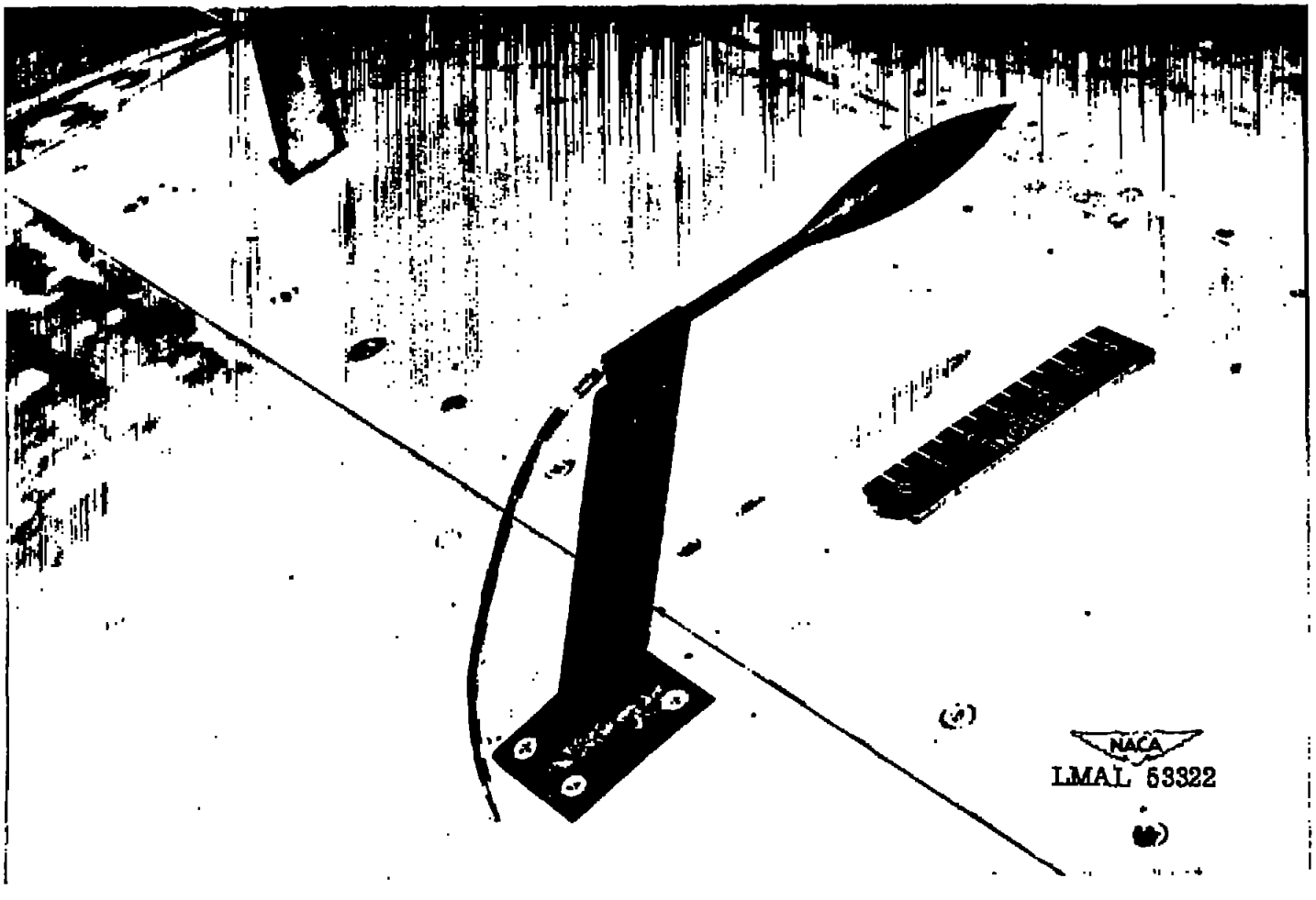

Figure 4.- Body-sting combination mounted on airplane wing.

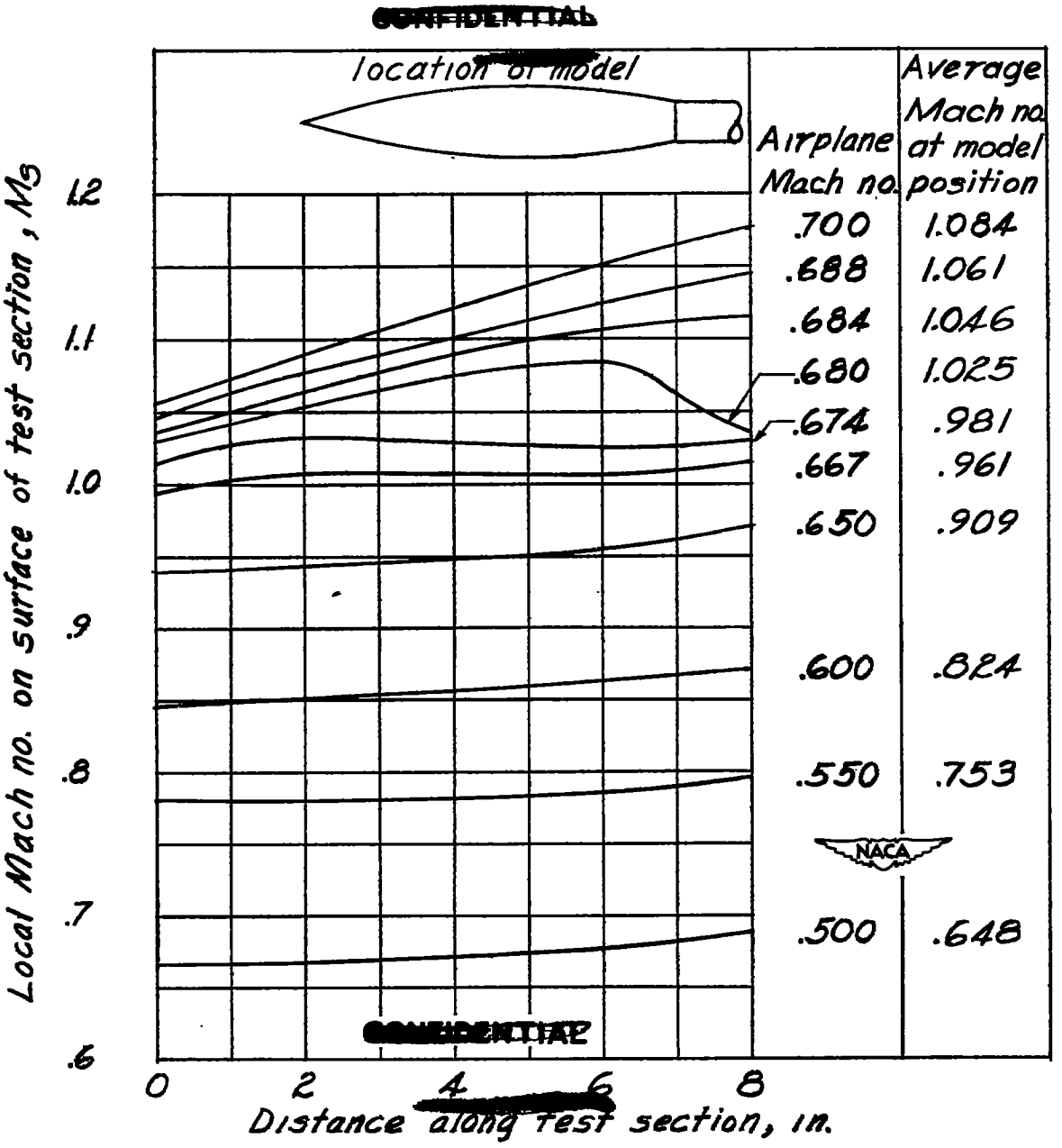

Figure 5.- Distribution of Mach no. on test section without model.

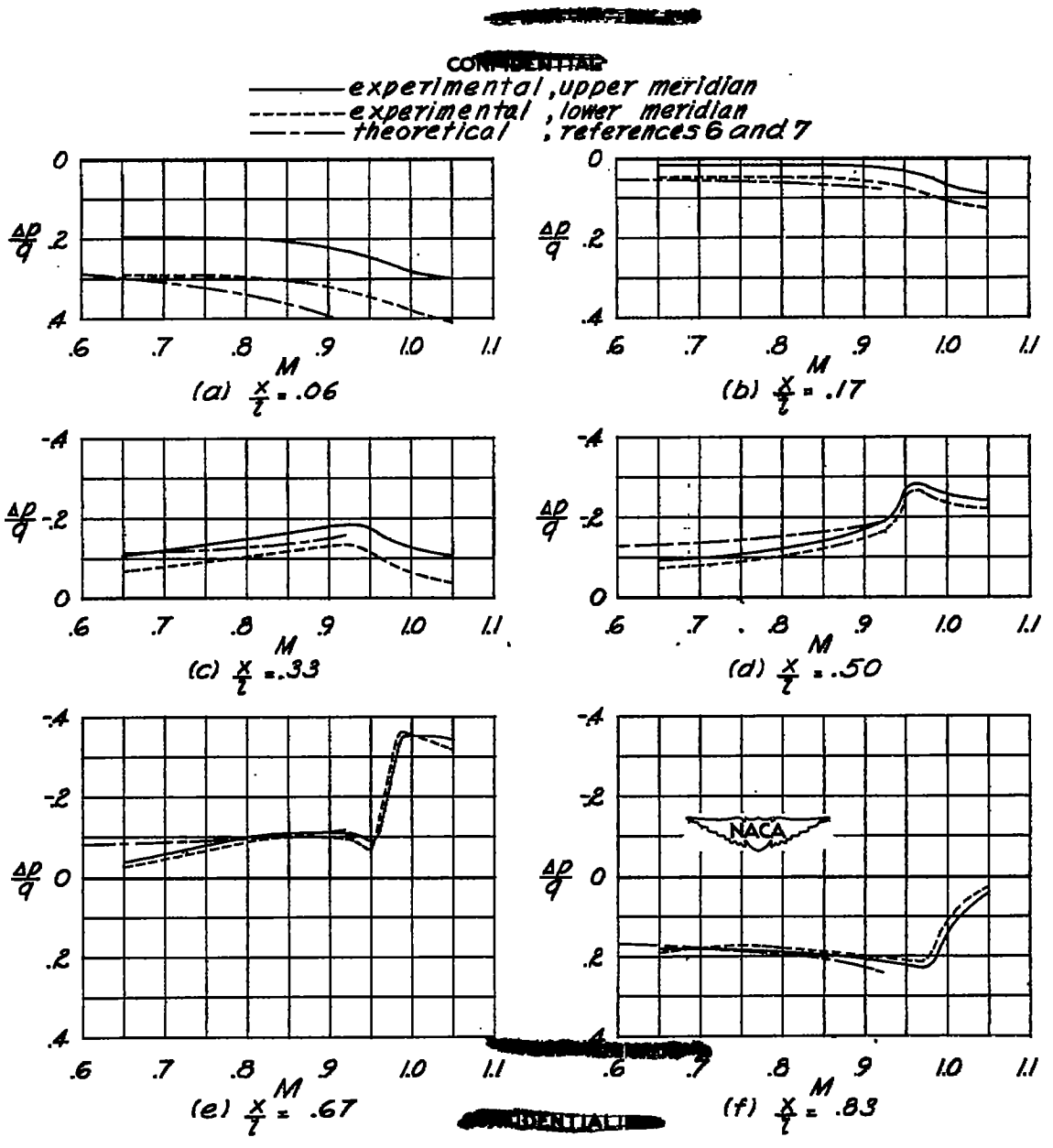

Figure 6.- Variation of $\frac{\Delta p}{q}$ with M at each orifice position; ½-inch diameter sting.

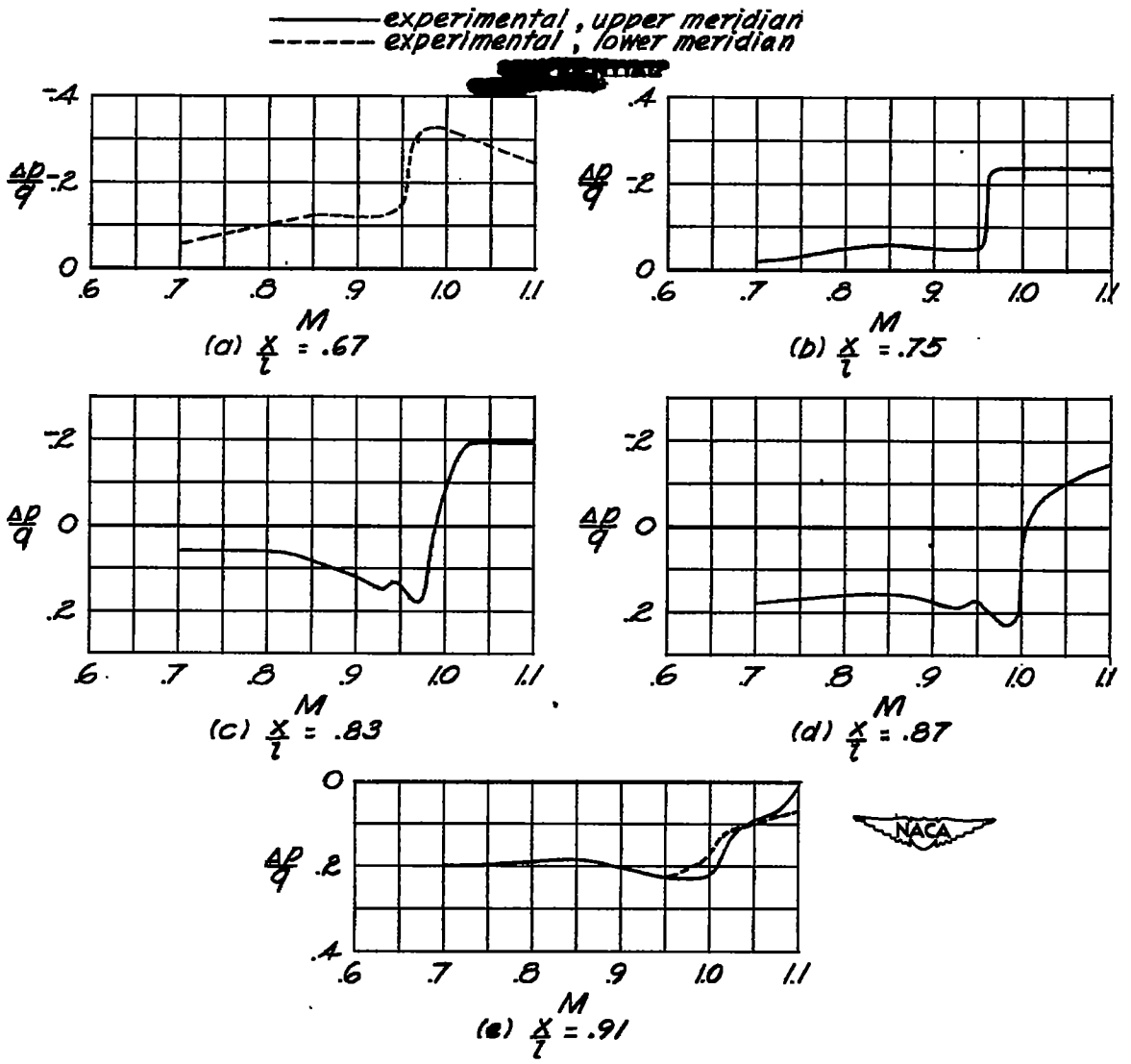

Figure 7.- Variation of $\frac{\Delta p}{q}$ with M at each orifice position; $\frac{1}{4}$-inch diameter sting.

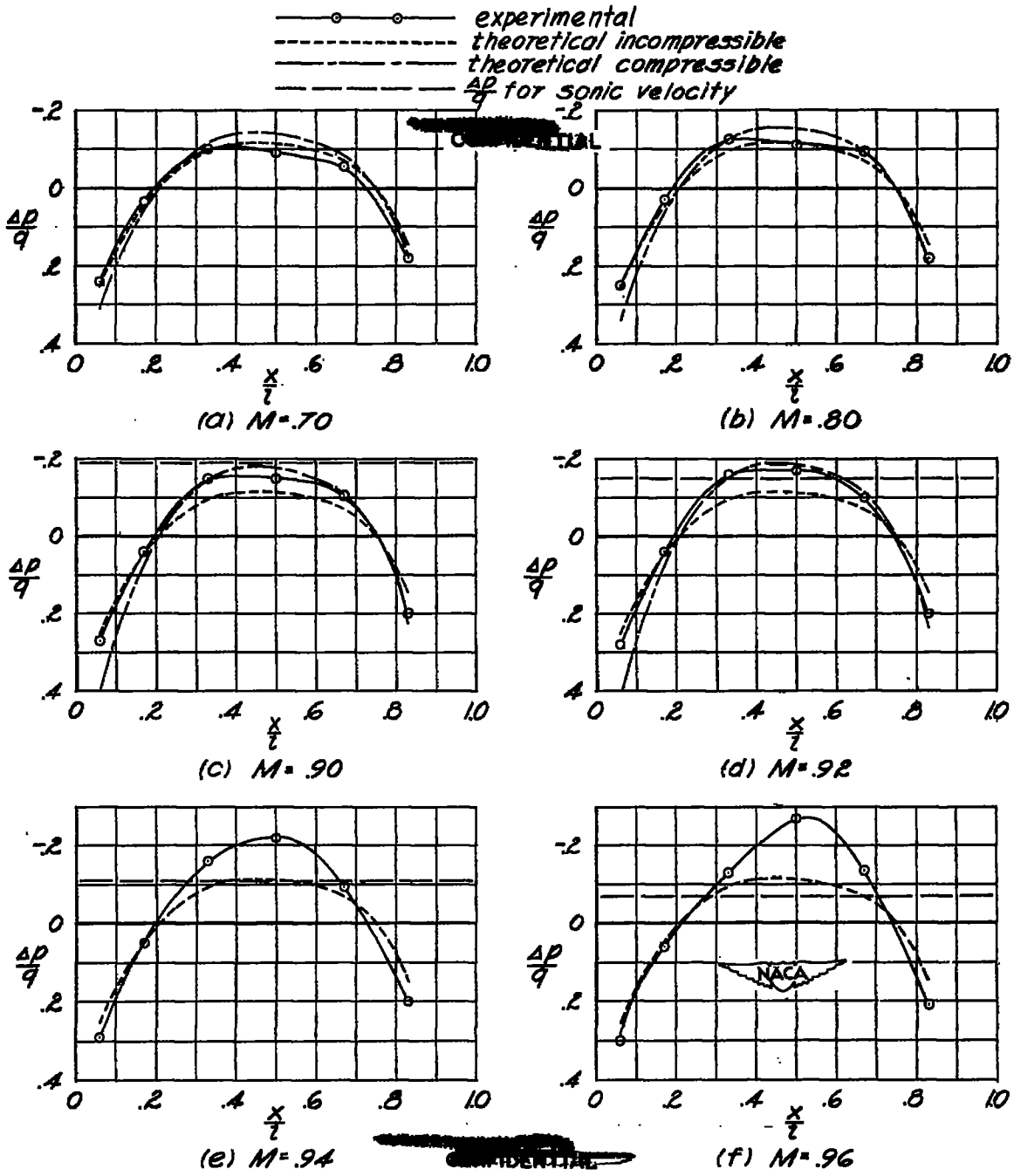

Figure 8.- Pressure distributions along axis for various Mach numbers; $\frac{1}{2}$-inch diameter sting.

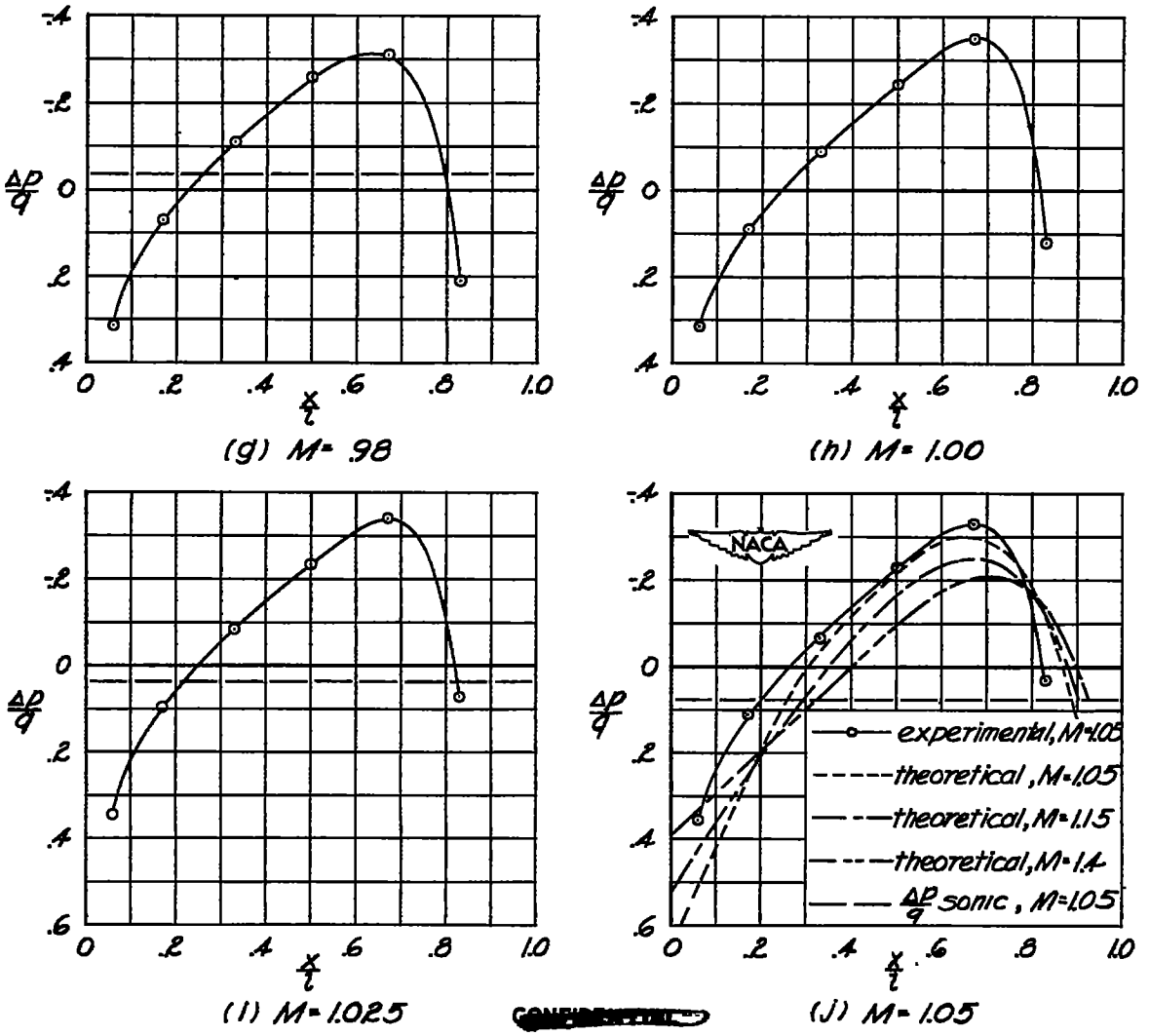

Figure 8.- Concluded.

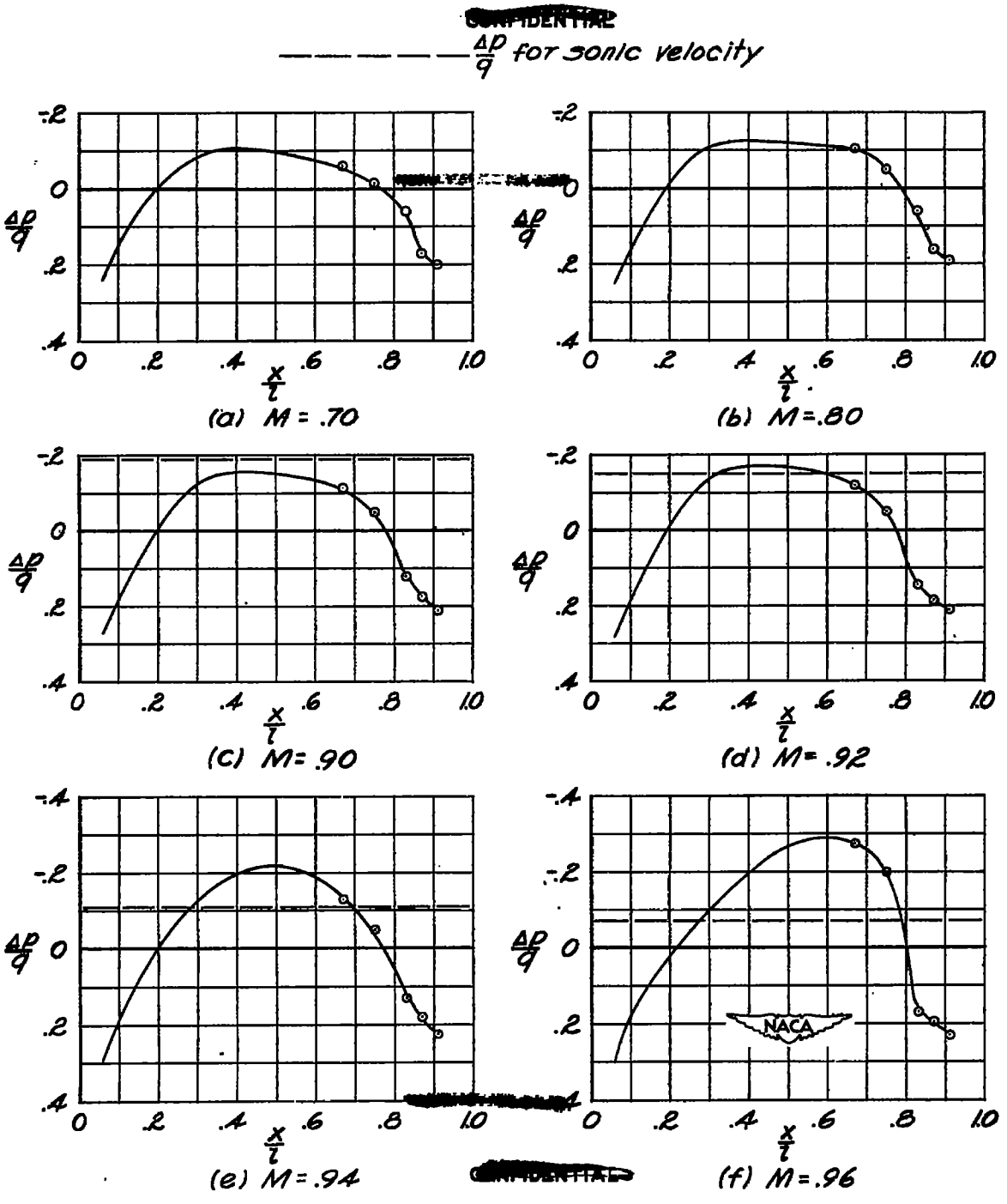

Figure 9.- Pressure distributions along axis for various Mach numbers; $\frac{1}{4}$-inch diameter sting.

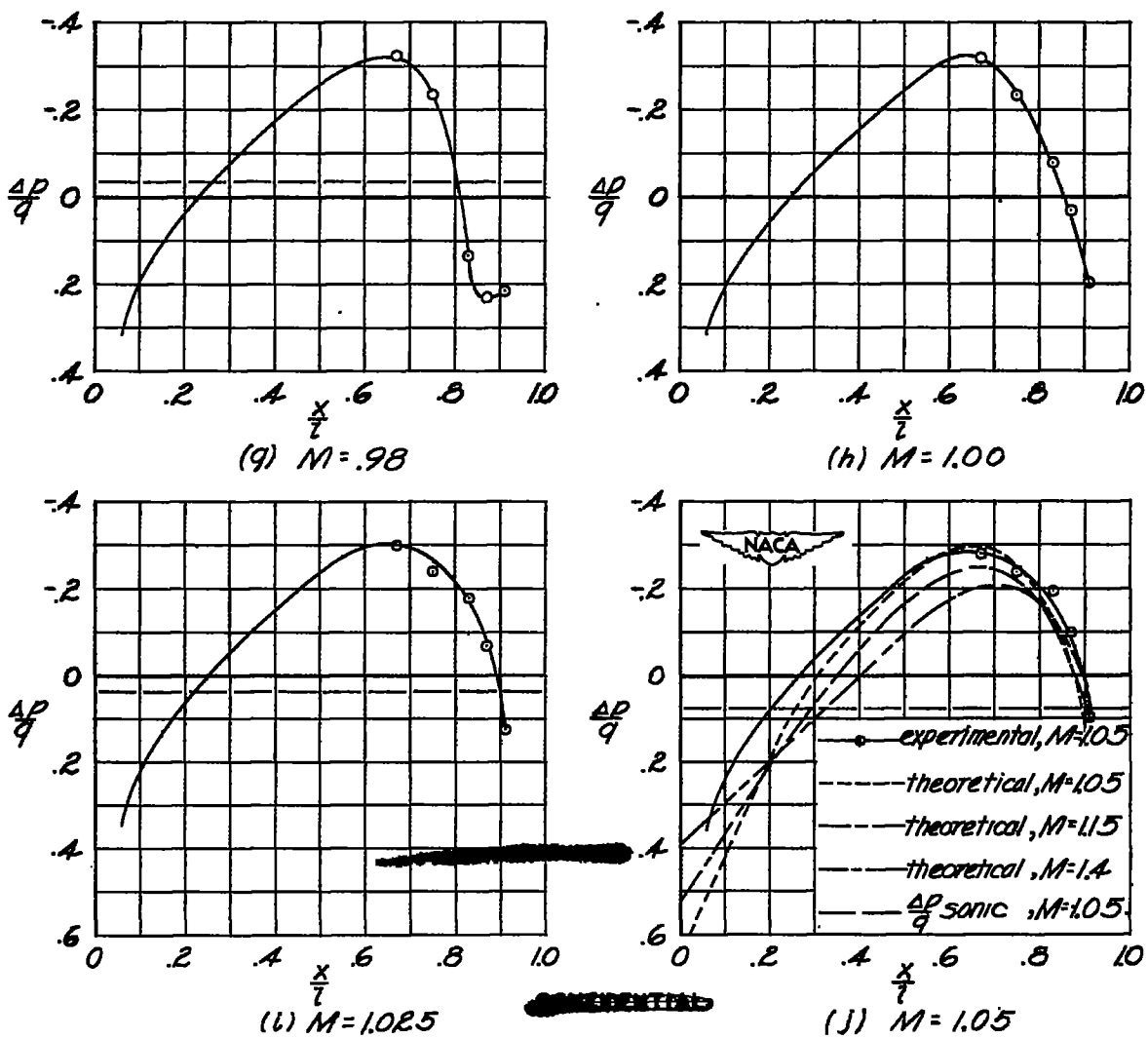

Figure 9.- Concluded.

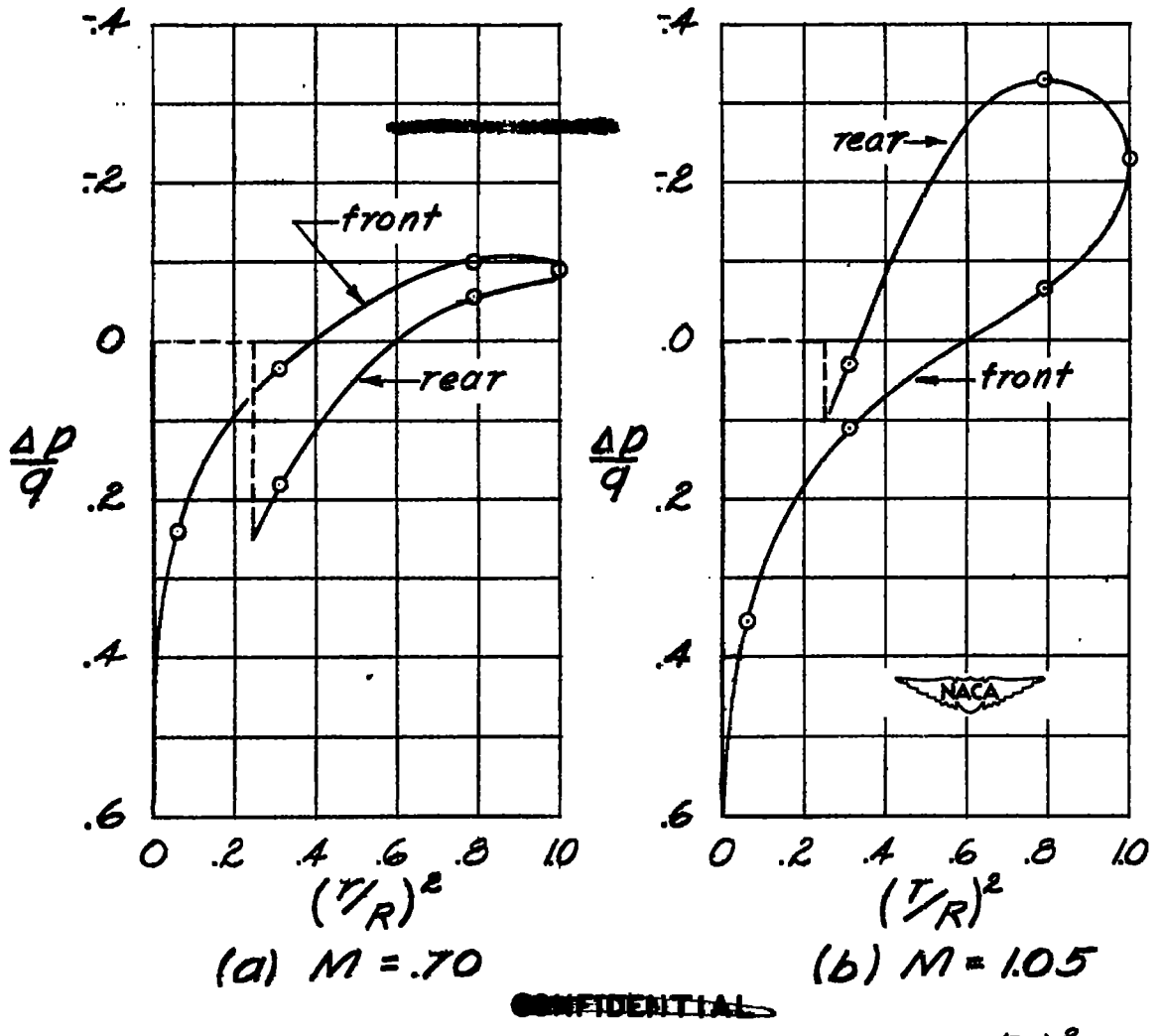

Figure 10.- Sample plots of $\frac{\Delta p}{q}$ vs. $\left(\frac{r}{R}\right)^2$ used in determining the value of the pressure-drag coefficient; $\frac{1}{2}$-inch diameter sting.

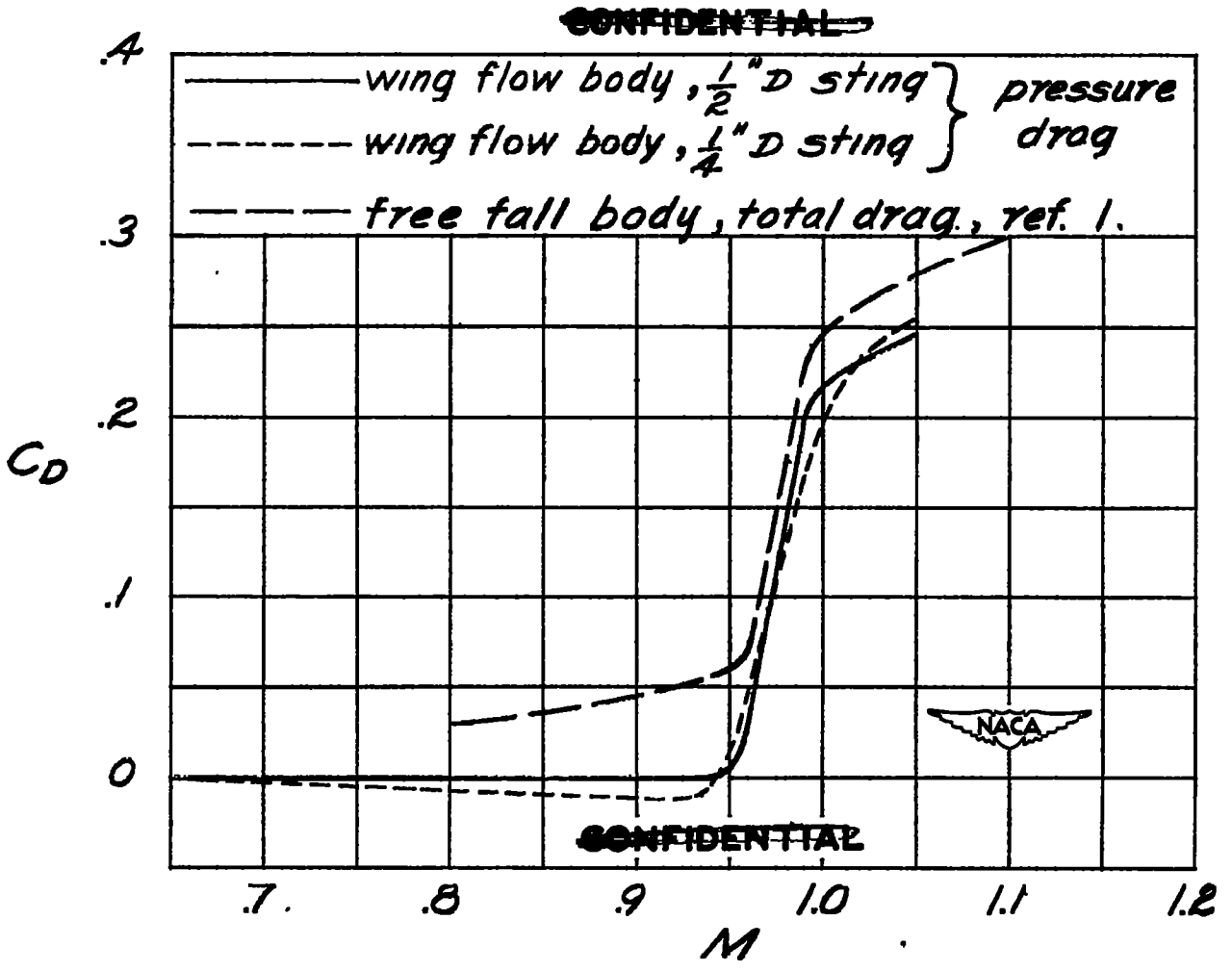

Figure 11.- Variation of C_D with M.